Materials Science and Engineering B108 (2004) 81–90

www.elsevier.com/locate/mseb

Cycle durability of Ca–Mg–Ni alloys and factors which cause degradation of hydrogen storage capacity

Hideaki Tanaka [a,*], Hiroshi Senoh [a], Nobuhiro Kuriyama [a], Kenji Aihara [b], Naoyoshi Terashita [c], Takuji Nakahata [d]

[a] *New Energy Carrier Research Group, Special Division for Green Life Technology, National Institute of Advanced Industrial Science and Technology (AIST), 1-8-31 Midorigaoka, Ikeda, Osaka 563-8577, Japan*

[b] *New Material Center attached to Osaka Science and Technology Center (OSTEC), 1-8-4 Utsubo-Hommachi, Nishi, Osaka 550-0004, Japan*

[c] *Japan Metals and Chemicals, Co., Ltd., 5-9-6 Toko-dai, Tsukuba, Ibaraki 300-2635, Japan*

[d] *Sumitomo Metal Industries, Ltd., 1-8 Fuso-cho, Amagasaki, Hyogo 660-0891, Japan*

Abstract

The cycle durability of Ca–Mg–Ni hydrogen storage alloys, which are investigated in the Japanese national project (International Clean Energy Network), WE-NET, was examined using pure H_2 (99.99999%). The tested alloys were $Ca_{0.25}Mg_{0.66}Y_{0.09}Ni_{1.86}$ (cubic $MgCu_2$-type structure), $Ca_{0.55}Mg_{0.45}Ni_3$ (rhombohedral $PuNi_3$-type) and $Ca_{0.5}Mg_{0.5}Ni_2$ ($MgCu_2$-type). Although initially the 'dynamic' hydrogen storage capacities were H/M ~0.7, they decreased steeply within a few cycles, and then they declined gradually. At around 400th cycle, they decreased to nearly half of the maximum capacities regardless of crystal structures and compositions of the tested alloys. However, their 'equilibrium' capacities did not decrease as the 'dynamic' ones with progress of hydrogen sorption. As for the bulk, not serious disproportionation but pulverization and lattice expansion were observed by X-ray diffractometry (XRD) and microscopic analyses. The expansion indicated that some amounts of hydrogen remained in the lattice cells. It was considered that pulverization of the alloy particles and amorphous shell formed on the surface prevented the alloys from smooth hydrogen sorption, and which led to the decrease of the 'dynamic' hydrogen storage capacities without that of the 'equilibrium' ones in the cycle tests.

Keywords: Ca–Mg–Ni alloy; Cycle durability; Dynamic hydrogen storage capacity; Equilibrium hydrogen storage capacity; Pulverization; Surface amorphization

1. Introduction

In Japan, the International Clean Energy Network using hydrogen, what we call, the WE-NET project has been carried out by the New Energy and Industrial Technology Development Organization (NEDO) and its cooperative organizations since 1993 [1–15]. The WE-NET is a large-scale project which will provide a solution to the global dilemma of producing and utilizing energy while simultaneously preserving the environment. One of the important purposes for research and development in the project is to aim at short- or mid-term realization of introducing hydrogen energy into society. Hydrogen absorbing materials have been expected to be promising storage media. To aim at an application to either mobile or stationary facilities, a hydrogen storage material having an effective hydrogen absorbing capacity of 3 wt.% or more, a hydrogen release temperature of 373 K or lower, and a storage capacity after 5000 cycles of 90% or more of the initial value, is developed since 1996 [9,14,16]. In the 2001 financial year, the numerical targets for hydrogen storage materials in this project were amended recently so that capacity is 5 wt.% and the temperature is 423 K in order to apply to vehicles [17]. Various kinds of hydrogen storage media such as alloys, carbonaceous materials and complex materials have been investigated for distributed storage and transportation. In a progress of the WE-NET project, some new and expectable materials such as Ca–Mg-, V- and Ti–Cr-based alloys were found out as promising the hydrogen storage alloys and hydrogenation properties were investigated. However, durability has hardly been concerned very much although an absorbing capacity and a releasing temperature were emphasized in the investigations hitherto.

* Corresponding author. Tel.: +81-72-751-9651; fax: +81-72-751-9629.

E-mail address: tanaka.hide@aist.go.jp (H. Tanaka).

0921-5107/$ – see front matter © 2003 Elsevier B.V. All rights reserved.
doi:10.1016/j.mseb.2003.10.106

Mg and Ca which are main components of Ca–Mg-based alloys have small densities (Mg: 1.74 g/cm^3, Ca: 1.55 g/cm^3) and they show excellent affinities for hydrogen and form hydrides, MgH_2 and CaH_2, easily. However, these hydrides are too stable to be applied to practical use. Some Mg- and Ca-based binary alloys with Ni such as Mg_2Ni [18] and $CaNi_5$ [19] are less stable hydride phases and they are well-known hydrogen storage alloys. According to the Mg–Ni [20], Ca–Ni [21], and Mg–Ca [22] binary phase diagrams, $MgNi_2$, $CaNi_2$, $CaNi_3$, Ca_2Ni_7, and $CaMg_2$ intermetallic compounds exist as other equilibrium phases besides the above two phases. But, although they can combine with large amount of hydrogen, the compounds are unsuitable for practical use because they form very stable hydrides or no hydrides. In addition, the hydrogenations are irreversible usually owing to disproportionation and so on. There are even no available phase diagrams [23] as to the Ca–Mg–Ni ternary system. Thus, the alloys except some pseudobinary Ca–Mg–Ni alloys were never investigated much.

We have investigated the Ca–Mg–Ni systems in the WE-NET project for several years and found out some new type of hydrogen storage materials [14,15,24,25]. Further, we discovered that it is sometimes effective to add rare-earth elements into the Ca–Mg–Ni alloy in order to improve hydrogenation properties and structural stability [26–28]. However, as for cycle durability of the Ca–Mg–Ni hydrogen storage alloys, the durability has been also considered to be unsuitable in practice derivatively from marked disproportionation often observed in some Ca–Mg, Mg–Ni and Ca–Ni binary and pseudobinary alloys although there is little experimental information on the cycle durability.

In this work, $Ca_{0.25}Mg_{0.66}Y_{0.09}Ni_{1.86}$ [28], $Ca_{0.5}Mg_{0.5}Ni_2$ [29] and $Ca_{0.55}Mg_{0.45}Ni_3$ [30,31] alloys are chosen from the Ca–Mg–Ni alloys and investigated concerning their hydrogenation properties through static and dynamic measurements. In addition, the alloys were investigated closely on bulk and surface states in order to ascertain the factors which cause change of properties with repetition of hydrogenation and dehydrogenation cycles.

2. Experimental

2.1. Sample preparation

The $Ca_{0.25}Mg_{0.66}Y_{0.09}Ni_{1.86}$ sample alloy was prepared by radio frequency induced melting and annealing at 1123 K for 24 h. The $Ca_{0.5}Mg_{0.5}Ni_2$ alloy was synthesized as follows: (1) sintering a preliminary pellet which consists of ready-made $CaNi_2$, Mg and Ni powders at 1073 K for 2 h in an Ar (purity: 99.995% up) atmosphere of 0.7 MPa, (2) crushing it, (3) re-pelletizing and sintering at 1173 K for 2 h in the same atmosphere. The $Ca_{0.55}Mg_{0.45}Ni_3$ alloy was synthesized by sintering from mixture of the above $Ca_{0.5}Mg_{0.5}Ni_2$, Mg and Ni through the same thermal history as sintering of the above $Ca_{0.5}Mg_{0.5}Ni_2$.

2.2. Cycle test

The cycle tests and the measurements of the pressure-composition (*P–C*) isotherms were carried out by use of an MH durability experimental system (manufactured by Japan Steel Works Co.) illustrated in Fig. 1. The sample autoclave

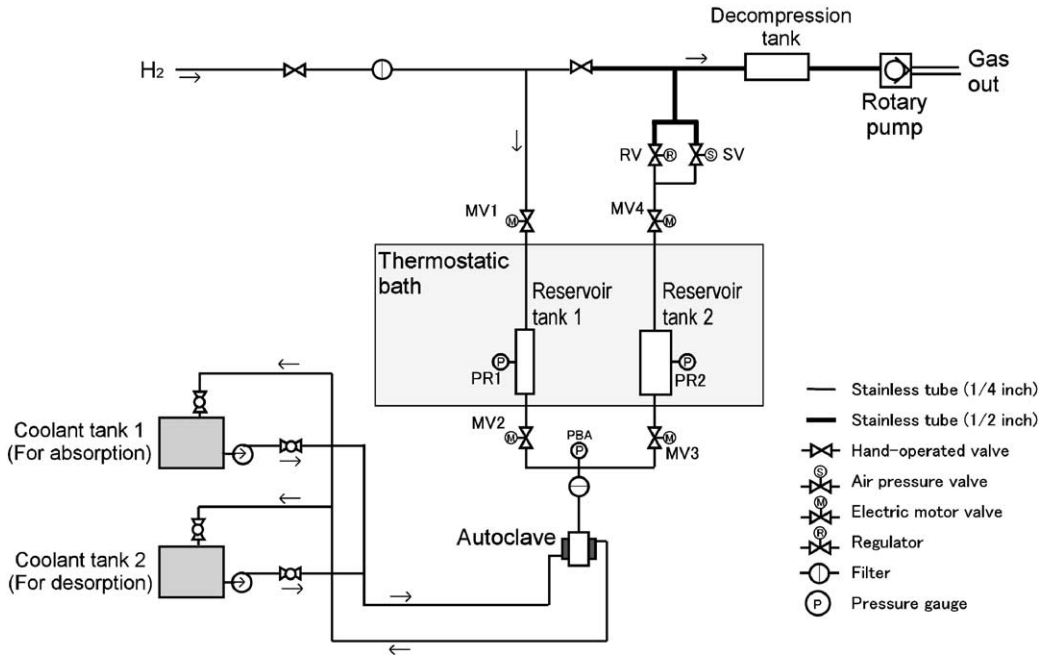

Fig. 1. Schematic figure of the MH durability testing system.

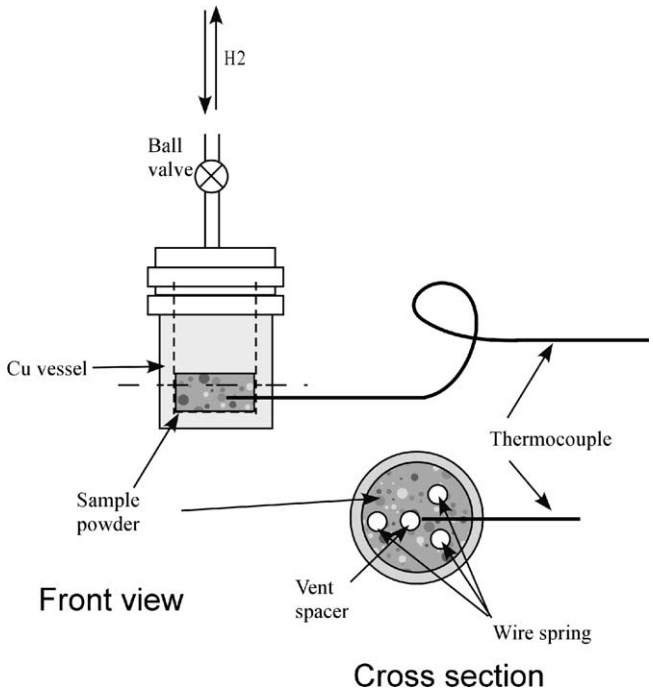

Fig. 2. Schematic diagrams of the sample autoclave for the series of the cycle tests.

is illustrated in Fig. 2. The autoclave can be separated from the system owing to a ball valve without exposing the sample to air. The recorded temperature is that of the samples themselves because the tip of the thermocouple was stuck into the sample powder in the autoclave as shown in Fig. 2. The testing conditions of the cycle test are shown in Table 1.

The durations were determined in consideration of the time when stationary state of H_2 pressure in the sample autoclave is indicated. Namely, equilibrium of hydrogenation/dehydrogenation was not considered here. The cycle tests were continued until the dynamic hydrogen storage capacities fall off to half of the maximum capacity recorded in the beginning of the testing process.

The *P–C* isotherms were measured at 293, 313, and 353 K after evacuation at 353 K in order to examine changes of the equilibrium properties of the samples immediately after initial-activation (after a few cycles of it, exactly), after 100th and 300th cycle and just before finishing of the cycle tests. Here, the number of the cycles for either *P–C* isotherm measurements or initial activation treatments were also counted as testing cycle numbers.

Table 1
Testing conditions

Gas purity (%)	99.99999
Absorbing duration (min)	30
Desorbing duration (min)	30
Absorbing pressure (MPa)	3
Desorbing pressure (MPa)	0 (evacuated)
Room temperature (K)	299
Sample temperature (K)	313

2.3. Analysis

The constituent phases and crystal structure of the original and tested sample alloys were identified by powder X-ray diffractometry (XRD: RINT2000® by Rigaku Co., Ltd.) by using Cu Kα X-ray. The tested samples were taken out from the autoclave in a glove box filled with Ar atmosphere of 0.1 MPa. The samples were mixed with liquid paraffin in order to prevent them from oxidization during measurement. The tested alloys were heated at 423 K for a few hours in the glove box before the XRD measurement.

Deformation such as microcracks and cleavage in the sample powders before and after the tests was observed by a scanning electron microscope (SEM: JSM-6301F® by JEOL Ltd.). The data observed by SEM were compared with results from a laser diffraction particle size analyzer (PSA: SALD-2000® by Simadzu Coop.). When the particle size was measured by PSA, the sample powders were mixed with a solution consisting of glycerin and ethanol, because they react on any water-based solvents which are used usually. Additionally, the $Ca_{0.25}Mg_{0.66}Y_{0.09}Ni_{1.86}$ sample particles before and after the tests were observed microscopically with a high resolution transmission electron microscope (HR-TEM: H-9000NA® by Hitachi Ltd.) in order to characterize each structure.

3. Results and discussion

Fig. 3 shows the degradation curves for $Ca_{0.25}Mg_{0.66}Y_{0.09}Ni_{1.86}$, $Ca_{0.5}Mg_{0.5}Ni_2$ and $Ca_{0.55}Mg_{0.45}Ni_3$. Regardless of the alloys' compositions, the dynamic hydrogen storage capacities decrease to half of the maximum capacity at around the 400th cycle. Through several cycles at the beginning, the dynamic capacities show a maximum, and then decline exponentially.

Fig. 4(a) to (c) show the change of *P–C* isotherms for the alloys at 313 K with cycle progress. It is perceived that the plateaus on the curves get steeper with increase of the

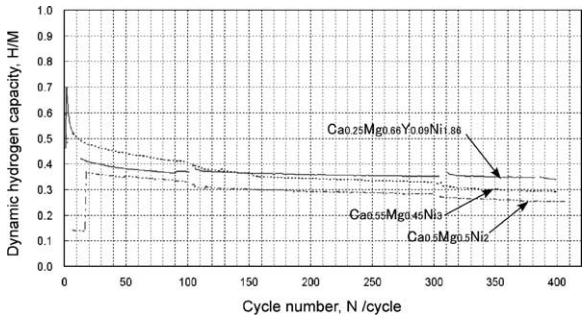

Fig. 3. Cycle degradation properties for $Ca_{0.25}Mg_{0.66}Y_{0.09}Ni_{1.86}$, $Ca_{0.5}Mg_{0.5}Ni_2$, and $Ca_{0.55}Mg_{0.45}Ni_3$.

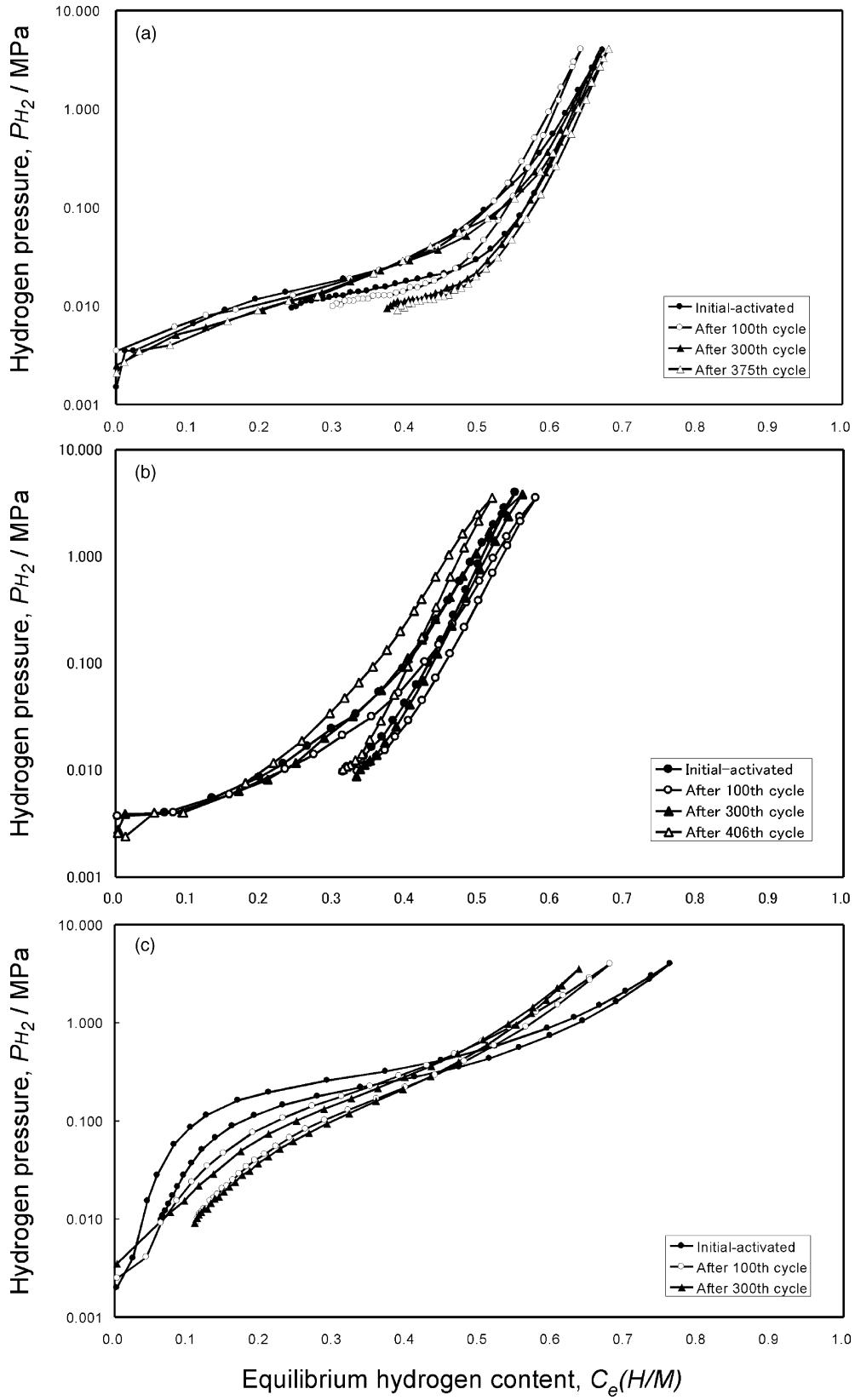

Fig. 4. *P–C* isotherms at 313 K for: (a) $Ca_{0.25}Mg_{0.66}Y_{0.09}Ni_{1.86}$, (b) $Ca_{0.5}Mg_{0.5}Ni_2$, and (c) $Ca_{0.55}Mg_{0.45}Ni_3$.

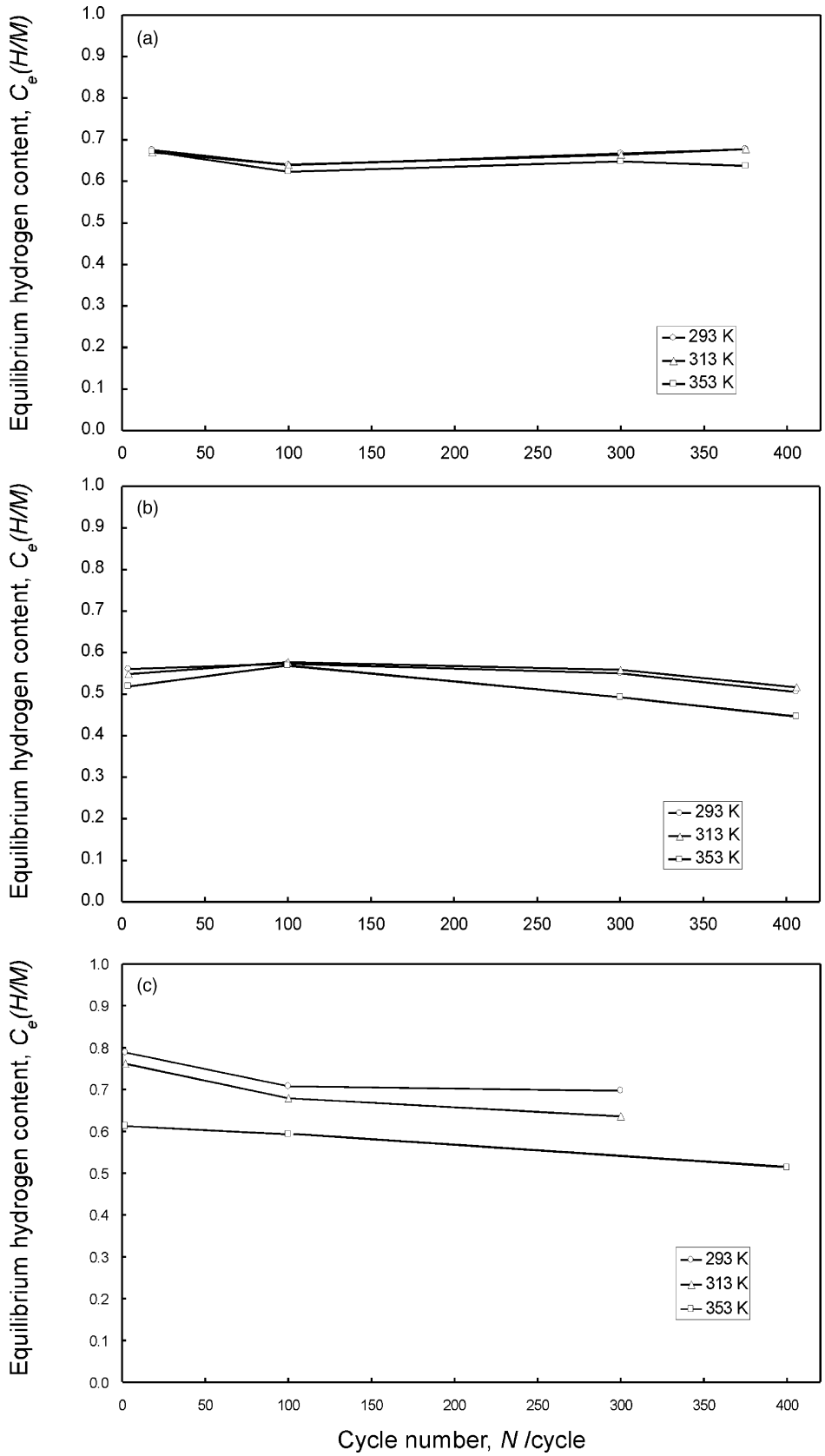

Fig. 5. Change in equilibrium hydrogen storage capacities with increase of cycle number: (a) $Ca_{0.25}Mg_{0.66}Y_{0.09}Ni_{1.86}$, (b) $Ca_{0.5}Mg_{0.5}Ni_2$, and (c) $Ca_{0.55}Mg_{0.45}Ni_3$.

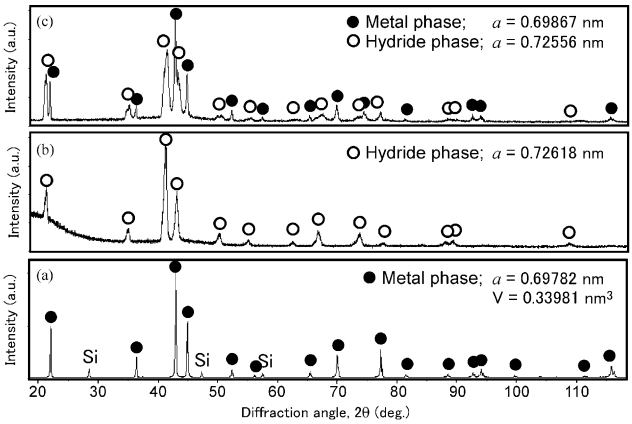

Fig. 6. X-ray diffraction profiles of $Ca_{0.25}Mg_{0.66}Y_{0.09}Ni_{1.86}$ before and after the series of the cycle test: (a) before the test, (b) as taken-out after 396 cycles, and (c) evacuated at 423 K for 2 h.

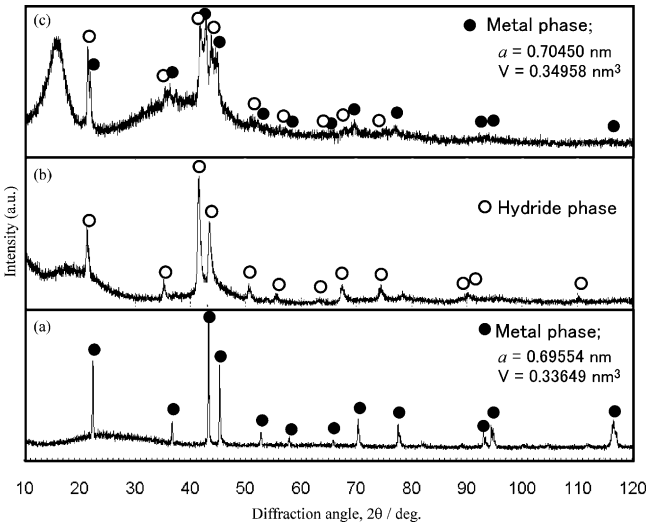

Fig. 7. X-ray diffraction profiles of $Ca_{0.5}Mg_{0.5}Ni_2$ before and after the series of the cycle test: (a) before the test, (b) as taken-out after 403 cycles, and (c) evacuated at 423 K for 2 h.

cycle number and the amounts of hoarded hydrogen increase gradually.

Fig. 5(a) to (c) show the relationship between equilibrium hydrogen storage capacities at 4 MPa and the cycle numbers for $Ca_{0.25}Mg_{0.66}Y_{0.09}Ni_{1.86}$, $Ca_{0.5}Mg_{0.5}Ni_2$ and $Ca_{0.55}Mg_{0.45}Ni_3$. Comparing Fig. 5 with Fig. 3, the 'dynamic' hydrogen storage capacities from cycle tests are smaller than the 'equilibrium' ones from the *P–C* isotherms for all three alloys. The hydrogen storage capacities seem small because equilibrium states were not achieved within 30 min. On the other hand, the equilibrium capacities hardly decrease although the dynamic ones decrease gradually.

Fig. 6 shows the X-ray diffraction profiles for $Ca_{0.25}Mg_{0.66}Y_{0.09}Ni_{1.86}$ before and after the cycle test. Not disproportionation but degradation of crystallinity is observed from the tested sample as shown in Fig. 6(b) and (c). The lattice seems to become amorphous or nano-crystalline structure in Fig. 6(c). Fig. 6(c) shows that a little expanding intermetallic compound phase and a hydride phase coexist even after the tested sample was heated at 423 K for 2 h. The lattice volumes of $Ca_{0.25}Mg_{0.66}Y_{0.09}Ni_{1.86}$ before and after the series of tests were $V = 0.33981$ and $0.34105\,nm^3$, respectively. The cell showed isotropic expansion with keeping the cubic $MgCu_2$-type structure. That, is, the cell volume expanded by +0.37%. This amount of expansion corresponds to that of hoarded hydrogen in the lattice cell. As shown in Fig. 7, $Ca_{0.5}Mg_{0.5}Ni_2$ did not give disproportionation but degradation of crystallinity after the test as well as the $Ca_{0.25}Mg_{0.66}Y_{0.09}Ni_{1.86}$, although they were synthesized with different processes. Both of $Ca_{0.5}Mg_{0.5}Ni_2$ before and after test show a cubic $MgCu_2$-type structure. The lattice volumes of the former and the latter were $V = 0.33649$ and $0.34958\,nm^3$. This stands for +3.9% expansion. $Ca_{0.55}Mg_{0.45}Ni_3$ with a rhombohedral $PuNi_3$-type structure was determined as $V = 0.3415\,nm^3$. It showed remarkable degradation with increase of cycle number. In fact, the *P–C* isotherms for only this alloy showed a remarkable change. It is known that this alloy is disproportionated in a hot H_2 atmosphere [31]. It is considered that this alloy was affected more especially by the hoarded or surrounding hydrogen than the others when it was heated at 353 K before the *P–C* isotherms measurements and/or instantaneous heating at hydrogenation during the cycle test process. It means that this alloy is less stable for hydrogen than the others and it is not so much worth investigating. Hereafter, it will be excluded from this study.

Figs. 8(a), (b) and 9(a) show the scanning electron microscope images and the differential particle size distribution for $Ca_{0.25}Mg_{0.66}Y_{0.09}Ni_{1.86}$ powder before and after the cycle test. The $Ca_{0.25}Mg_{0.66}Y_{0.09}Ni_{1.86}$ powder was sifted into the size from 75 to 150 μm by use of Japanese industrial standard (JIS) sieves before the cycle test. There are observed numerous pores not cracks in the particles before the test. However, we can see a lot of cracks not the pores in the tested particles. It is suggested that the pores may be the starting point of cracks and disappear gradually. The median diameter of the powder which was introduced by granular fracture through volume expansion and reduction during the cycle test was 22.984 μm. Figs. 8(c), (d) and 9(b) show the SEM images and the differential particle size distribution for $Ca_{0.5}Mg_{0.5}Ni_2$ before and after the cycle test. Virgin powder was flaky and had a coherent structure because it was prepared by a sintering process from a few kinds of raw material powders. This powder was also crushed and sifted by use of the JIS sieves before the test as well as $Ca_{0.25}Mg_{0.66}Y_{0.09}Ni_{1.86}$. Although distribution of the particle size was divided into a few gradations in the initial state, finally it was gathered around only one peak. Median diameter decreased from 43.377 to 21.994 μm. The tested particles showed flatter surfaces than the virgin ones. As a result of PSA for the sample alloy particles, pulverization was observed from one hundred odd micrometers to about 20 μm.

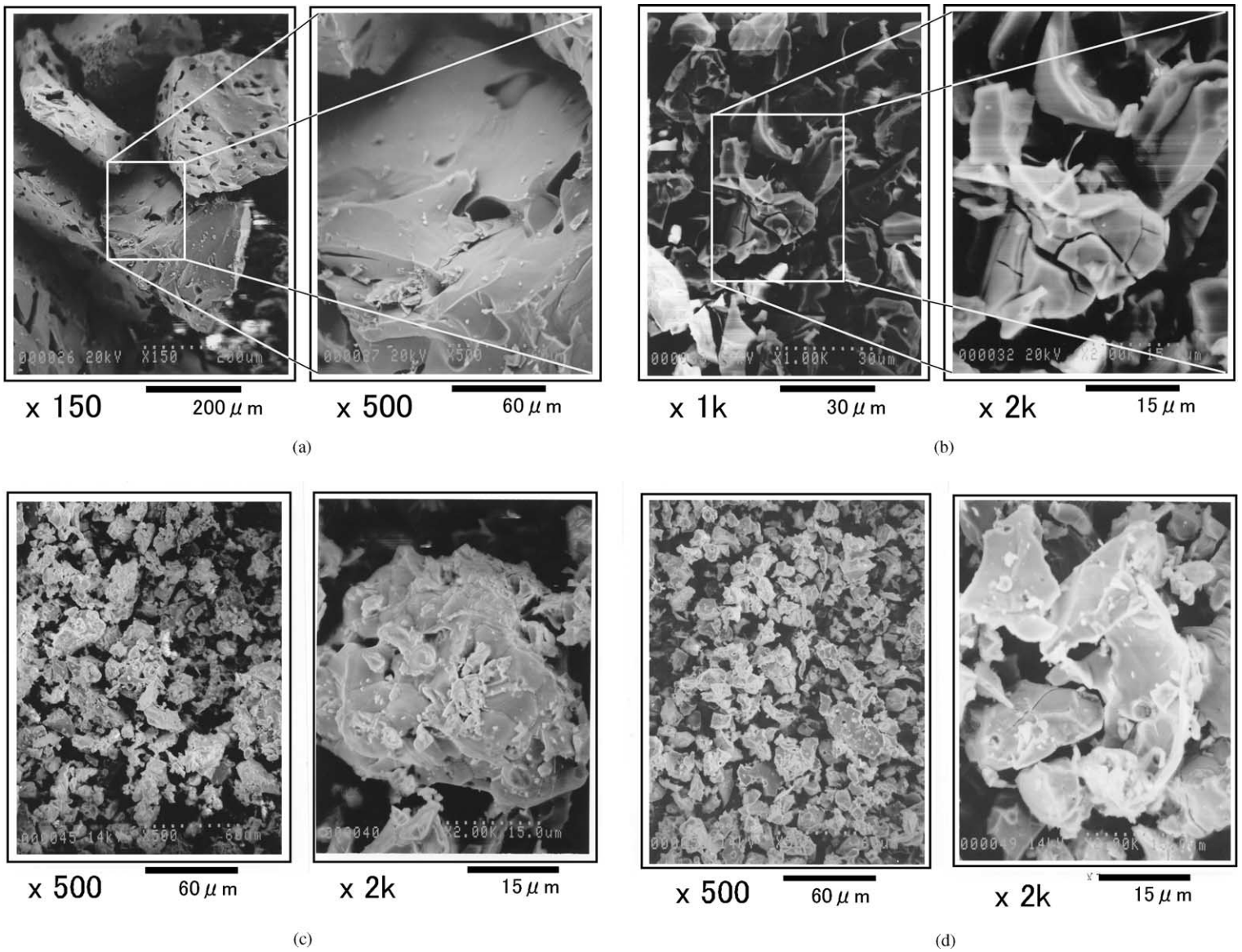

Fig. 8. Scanning electron microscopic (SEM) images: (a) virgin, (b) tested $Ca_{0.25}Mg_{0.66}Y_{0.09}Ni_{1.86}$, (c) virgin, and (d) tested $Ca_{0.5}Mg_{0.5}Ni_2$.

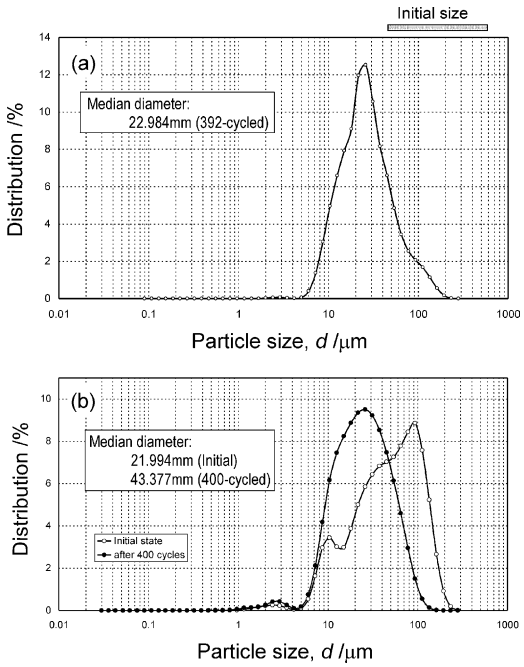

Fig. 9. Particle size distribution of the samples before and after the cycle tests: (a) $Ca_{0.25}Mg_{0.66}Y_{0.09}Ni_{1.86}$, and (b) $Ca_{0.5}Mg_{0.5}Ni_2$.

Fig. 10(a) and (b) show the TEM images and the selected area diffraction patterns of $Ca_{0.25}Mg_{0.66}Y_{0.09}Ni_{1.86}$ before the cycle test. Surface area is crystalline and habit plane {1 1 1} crops out. The diffraction pattern shows coexistence of amorphous structure and the crystalline structure. Fig. 10(c) and (d) show those degraded after the cycle test. Crystalline structure is covered with amorphous shell and the rugged surface as observed in (a) is not formed. Amorphous structure was observed in either (b) or (d), but the diffraction ring from the degraded particle is clearly broader than that from the virgin particle. In addition, we observe a certain disproportionation during the cycle test because there are quite different diffraction spots in Fig. 10(d). On the other hand, dislocation is also observed at the lower left part of the image. It is considered that it is induced during the cycle because it is not observed in the image before the test.

The dynamic hydrogen storage capacities of $Ca_{0.25}Mg_{0.66}Y_{0.09}Ni_{1.86}$, $Ca_{0.5}Mg_{0.5}Ni_2$, and $Ca_{0.55}Mg_{0.45}Ni_3$ showed very similar degradation curves. On the contrary, the equilibrium capacities did not degrade so much as the dynamic ones. This tendency was common for all sample alloys

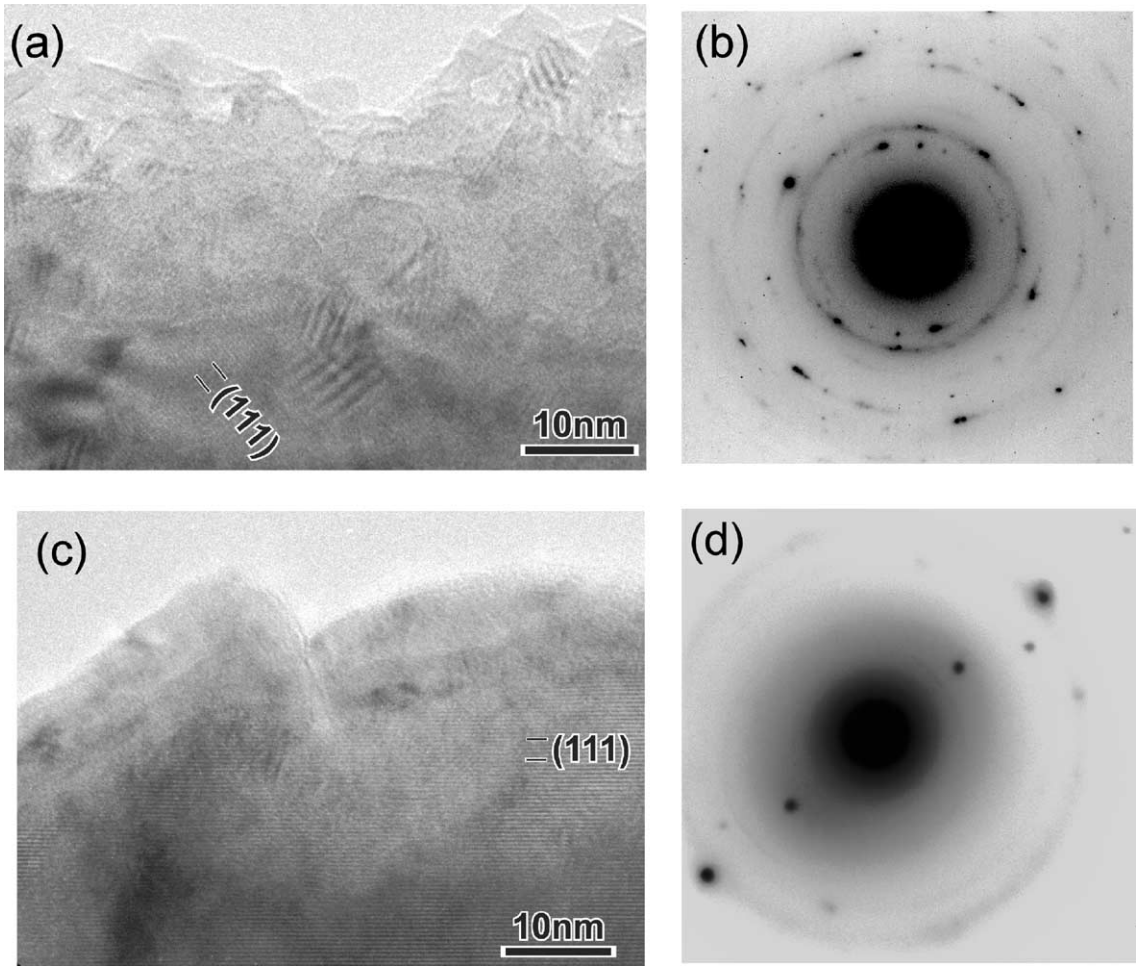

Fig. 10. High resolution transmission electron microscopic images and selected area diffraction patterns of the $Ca_{0.25}Mg_{0.66}Y_{0.09}Ni_{1.86}$ particles before and after the cycle tests: (a) and (b) show morphology and pattern before the test, (c) and (d) show those after the test.

regardless of differences in composition, crystal structure, and preparing method, which means that hydrogen mobility is an important factor for the cycle durability. It is considered that the capacity degradation was inconspicuous because the equilibrium capacity is independent of the sorbing duration. However, the dynamic capacity depends on the duration due to decrease of the mobility, which lead to lessen the capacity. As a result of analyses with a microscopic viewpoint, these phenomena are so similar to conventional consideration which is introduced from the data on the other Ca–Ni–based alloys [32].

4. Conclusion

Cycle durability on repetition of the hydrogen absorption and desorption was examined through pressure cycle tests for three kinds of Ca–Mg–Ni alloys: $Ca_{0.25}Mg_{0.66}Y_{0.09}Ni_{1.86}$, $Ca_{0.5}Mg_{0.5}Ni_2$, and $Ca_{0.55}Mg_{0.45}Ni_3$. In addition, the intrinsic degradation factors were investigated microscopically and crystallographically. The 'dynamic' hydrogen storage capacities of the alloys from the cycle tests decreased to half the maximum capacities during around 400 cycles of hydrogen sorption. On the other hand, the 'equilibrium' capacities from the *P–C* isotherms did not change so much at low temperature, in particular. However, the alloys were liable to be affected by the heat of hydrogenation or hot coolant. So far as the isotherms show, $Ca_{0.55}Mg_{0.45}Ni_3$ was influenced particularly. As a result of SEM observations for $Ca_{0.25}Mg_{0.66}Y_{0.09}Ni_{1.86}$, numerous cracks were induced in the particles and they were pulverized gradually during the cycling. But the sintered $Ca_{0.5}Mg_{0.5}Ni_2$ also was pulverized but cracks were not induced. The TEM images show that the degraded particles consist of the crystalline core and the amorphous thin shell and that they contain dislocations. Thus, amorphization and accumulation of lattice defects have often been mentioned as convincing degradation factors. We can not still conclude precisely why the shell was formed and its influence on hydrogen absorption properties. However, it is possible that the shell is the structure affected by heat during hydrogenating or a certain hydrogenated structure. In addition, the particle size reduction which results in median diameters of about 22 μm during the cycle progress should be studied in more detail.

These Ca–Mg–Ni alloys show smaller hydrogen storage capacities, either 'dynamic' or 'equilibrium', than conventional hydrogen storage alloys such as rare-earth-, Ti-, and Mg-based ones. But the equilibrium capacity did not degrade so much. The alloys have the potential for a longer life if we apply a mild operating conditions. This series of alloys should be further studied in order to improve the structural degradation during cycling. The WE-NET project is over, but we are expecting that the overall hydrogen storage characteristics of these alloys will be investigated more detailed in a succeeding project.

Acknowledgements

We wish to express our great thanks for the working support by Dr. Satoshi Ichikawa (AIST, TEM observation and discussion thereof), Mrs. K. Hamaguchi (AIST, SEM operation), Mr. A. Taniguchi (Kansai University, Thermal analysis) and Mr. D. Takasugi (Staff Japan Co., Ltd., Particle size analysis).

References

[1] H. Tamura, I. Uehara, Y. Osumi, T. Sakai (Eds.), Hydrogen Storage Alloys—Fundamentals and Frontier Technologies, NTS, 1998, pp. 371–375.
[2] S. Katayama, The Most Advanced Technology for Hydrogen Energy, in: T. Ohta (Ed.), NTS, 1995, p. 674.
[3] C. Hamaguchi, Clean Energy 5 (1) (1996) 72–75.
[4] K. Fukuda, Clean Energy 5 (2) (1996) 69–72.
[5] S. Ohkura, Clean Energy 5 (3) (1996) 74–79.
[6] K. Ikoma, Clean Energy 5 (4) (1996) 76–79.
[7] A. Fujitani, Clean Energy 5 (5) (1996) 58–60.
[8] E. Kawagoe, Clean Energy 5 (6) (1996) 59–63.
[9] E. Akiba, Clean Energy 5 (7) (1996) 58–61.
[10] J. Hama, Clean Energy 5 (8) (1996) 58–62.
[11] N. Iketani, Clean Energy 5 (10) (1996) 59–62.
[12] M. Watanabe, Clean Energy 5 (11) (1996) 56–61.
[13] WE-NET, 1st phase R&D, Interim Report, Issued by NEDO, 1997.
[14] WE-NET Annual Report, Subtask 5, R&D for Hydrogen Transportation and Storage Technology, Fifth chapter, R&D of Hydrogen Storage Alloys for Hydrogen Distributed Transportation and Storage, Issued by NEDO and ENAA (Every year from 1994 to 1998).
[15] WE-NET Annual Report, Task 11, Phase II, R&D of Hydrogen Storage Alloys for Hydrogen Distributed Transportation and Storage, Issued by NEDO and OSTEC (Every year from 1999 to 2002).
[16] Promotion Pamphlet, International Clean Energy Network Using Hydrogen (WE-NET), Phase II Program, Issued by NEDO, 2000.
[17] WE-NET Annual Report, Task 11, Phase II, R&D of Hydrogen Storage Materials, Issued by NEDO and OSTEC, 2003.
[18] J.J. Reilly, R.H. Wiswall Jr., Inorg. Chem. 7 (1968) 2254.
[19] G.D. Sandrock, J.J. Murray, M.L. Post, J.B. Taylor, Mater. Res. Bull. 17 (1982) 887–894.
[20] T.B. Massalski, H. Okamoto, P.R. Subramanian, L. Kacprzak (Eds.), Binary Alloy Phase Diagrams, second ed., ASM International, 1996, p. 2529.
[21] T.B. Massalski, H. Okamoto, P.R. Subramanian, L. Kacprzak (Eds.), Binary Alloy Phase Diagrams, second ed., ASM International, 1996, p. 936.
[22] T.B. Massalski, H. Okamoto, P.R. Subramanian, L. Kacprzak (Eds.), Binary Alloy Phase Diagrams, second ed., ASM International, 1996, p. 925.
[23] P. Villars, A. Prince, H. Okamoto (Eds.), Handbook of Ternary Alloy Phase Diagrams, ASM International, 1997, p. 7520.
[24] K. Kadir, T. Sakai, I. Uehara, L. Eriksson, J. Alloys Compd. 284 (1999) 145–154.
[25] N. Terashita, K. Kobayashi, T. Sasai, E. Akiba, J. Alloys Compd. 327 (2001) 275.
[26] K. Kadir, T. Sakai, I. Uehara, J. Alloys Compd. 287 (1999) 112–117.

[27] K. Kadir, T. Sakai, I. Uehara, J. Alloys Compd. 302 (2000) 264–270.
[28] N. Terashita, T. Sasai, E. Akiba, Kinzoku 72(6) 53–57.
[29] T. Nakahata, H. Maeda, K. Yonemura, N. Terashita, S. Takahashi, T. Sasai, Japan Patent, Published No. 2002-97535 (2002).
[30] T. Nakahata, H. Maeda, K. Yonemura, Japan Patent, Published No. 2001-303160 (2001).
[31] A. Taniguchi, Graduation Thesis, Kansai University, 2003.
[32] T. Kabutomori, H. Takeda, Y. Wakisaka, K. Ohnishi, J. Jpn. Inst. Met. 59 (1995) 219–228.